Anti-angiogenic Potential of VEGF Blocker Dendron-laden Gellan Gum Hydrogels for Tissue Engineering Applications

Valeria Perugini[1], Anna L. Guildford[1], Joana Silva-Correia[2-3], Joaquim M. Oliveira[2-3], Steven T. Meikle[1], Rui L. Reis[2-3], Matteo Santin[1,*]

[1]Brighton Studies in Tissue-mimicry and Aided Regeneration, Brighton Centre for Regenerative Medicine, School of Pharmacy and Biomolecular Sciences, University of Brighton, Brighton, UK.

[2]3B's Research Group–Biomaterials, Biodegradables and Biomimetics, University of Minho, Headquarters of the European Institute of Excellence on Tissue Engineering and Regenerative Medicine, AvePark, Parque de Ciência e Tecnologia, Zona Industrial da Gandra, 4805-017 Barco, Guimarães, Portugal.

[3]ICVS/3B's–PT Government Associate Laboratory, Braga/Guimarães, Portugal.

[*]*Corresponding author*: Prof. Matteo Santin

Address: Brighton Studies in Tissue-mimicry and Aided Regeneration, Brighton Centre for Regenerative Medicine, School of Pharmacy and Biomolecular Sciences, University of Brighton, Brighton, UK. Tel: +44 (0)1273 642083; *E-mail address:* m.santin@brighton.ac.uk

Running headline: Anti-angiogenic Potential of VEGF Blocker Dendron-laden GG Hydrogels

This article has been accepted for publication and undergone full peer review but has not been through the copyediting, typesetting, pagination and proofreading process which may lead to differences between this version and the Version of Record. Please cite this article as doi: 10.1002/term.2340

Abstract

Damage of non-vascularised tissues such as cartilage and cornea can result in healing processes accompanied by a non-physiological angiogenesis. Peptidic aptamers have recently been reported to block the vascular endothelial growth factor (VEGF). However, the therapeutic applications of these aptamers is limited due to their short half-life *in vivo*. In this work, an enhanced stability and bioavailability of a known VEGF blocker aptamer sequence (WHLPFKC) was pursued through its tethering of molecular scaffolds based on hyperbranched peptides, the poly(ε-lysine) dendrons, bearing three branching generations. The proposed design allowed simultaneous and orderly-spaced exposure of sixteen aptamers per dendrimer to the surrounding biological microenvironent, as well as a relatively hydrophobic core based on di-phenylalanine aiming to promote an hydrophobic interaction with the hydrophobic moieties of ionically-crosslinked metacrylated gellan gum (iGG-MA) hydrogels. The VEGF blocker dendrons were entrapped in iGG-MA hydrogels and their capacity to prevent endothelial cell sprouting was assessed qualitatively and quantitatively using 3D *in vitro* models and the *in vivo* chick chorioallantoic membrane (CAM) assay. The data demonstrate that at nanoscale concentrations, the dendronised structures were able to enhance control of the biological actvity of WHLPFKC at the material/tissue interface and hence the anti-angiogenic capacity of iGG-MA hydrogels not only preventing blood vessel invasion, but also inducing their regression at the tissue/iGG-MA interface. The *in ovo* study confirmed that iGG-MA functionalised with the dendron VEGF blockers do inhibit angiogenesis by controlling both size and ramifications of blood vessels in proximity of the implanted gel surface.

Keywords

Tissue regeneration, angiogenesis, anti-angiogenesis peptide, dendron, gellan gum, vascular endothelial growth factor.

1. Introduction

The invasion of healthy joint and intervertebral disc cartilage by fibrous tissue in pathological conditions such as osteoarthritis and rheumatoid arthritis as well as in traumatic and degenerative conditions is a consquence of abnormal angiogenesis (Pulsatelli *et al*., 2013). Pathological angiogenesis is linked by biochemical signalling to the insurgence of the inflammation causing the progressive degeneration of cartilage (Bonnet and Walsh, 2005). In clinics, non-steroidal anti-inflammatories drugs are administred to control inflammation and minimise joint damage, but these treatments neither improve the overall quality of life of the patient nor favour the repair of the degenerated tissue. The pathogenesis of other inflammatory disorders including synovial joints (Troken *et al*., 2007) and macular degeneration (AMD) (Xu *et al*., 2013) have also been associated to pathological angiogenesis, but appropriate therapies have not yet been identified (Carmeliet, 2003). However, it is widely accepted that drugs such as Sorafenib (Nexavar, Bayer) and Bevacizumab (Avastin^{TM}, Genentech), acting directly on the prime driver in the process of blood vessel sprouting, i.e. the vascular endothelial growth factor (VEGF), have been sucessfully used to control angiogenesis (Bischoff and Griffioen, 2008). Indeed, clinical therapies commonly target VEGF either to decrease its levels or to block its activation and any subsequent downstream signaling pathway (Kim *et al*., 2011). It has also been ascertained that the therapeutic efficacy of the various VEGF blockers available can be improved only by ensuring: (i) directed targeting of the effect of the blocker on endothelial cells (ECs) and (ii) the increased *in situ* retention of the blocker protracting the effect in the degenerated tissue (Wang, 2003).

To this end, the search for new anti-angiogenic agents of enhanced therapeutic efficacy has more recently been directed towards aptamers. Aptamers are oligonucleotides such as ribonucleic acid (RNA) and single-strand deoxyribonucleic acid (ssDNA) who have shown

high binding affinitiy towards a wide range of extra- and intracellular molecular targets (e.g. proteins, peptides or even cells) (Tuerk and Gold, 1990). Among them, synthetic peptidic aptamers have shown greater value in the treatment of vascular disorders (e.g. WHLPFKC sequence) (Erdag et al., 2007), but their clinical use is restricted by their relatively short half-life in vivo (Nugent and Edelman, 2003) In the pursuit of enhancing their retention time in target tissues and anti-angiogenic effects, dendrons ensuring a multiple and spacially-ordered presentation of of the anti-angiogenic linear VEGF blocker peptide WHLPFKC have previously been investigated (Meikle *et al*., 2011). The rationale in the design of such a type of poly-(ε-lysine) [K] dendron of third generation [Gen_3] was to expose simultaneously to the biological microenvironment a high number (16 per dendrons) of WHLPFKC and to increase the stability and interactions of this new anti-VEGF aptamer within the tissue extracellular matrix and/or at the surface of a biomaterial through the integration at the molecular root of a di-phenilalanine root [FF]. These VEGF blocker dendrons, named as $FFGen_3K(WHLPFKC)_{16}$ have provided evidence of anti-proliferative and apoptotic effects on human umbelical vascular endothelial cells (HUVEC) as well as inhibitory effect on their sprouting in *in vitro* models (Meikle *et al*., 2011).

These findings appear to offer future therapeutic opportunities when combined with the recent discovery of the properties of a novel hydrogels, the ionic-crosslinked methacrylated gellan gum (iGG-MA) hydrogels that was firstly described by Silva-Correia *et al*. (2011; 2012a-b; 2013a-b). The effects of combining the iGG-MA hydrogel discs with $FFGen_3K(WHLPFKC)_{16}$ has recently been studied in an ovine nucleotomy model showing a significant improvement in the regeneration of tissues with physicological features (Reitmaier *et al*., 2014).

The present study aims to demonstrate the high level of control over angiogenesis offered by iGG-MA hydrogels loaded with the VEGF blocker dendrons. It compares the efficacy of this

new VEGF blocker dendrons to the linear WHLPFKC sequence by firstly an *in vitro* three dimensional (3D) EC sprouting test and later validated by an *in ovo* model. At a relatively low therapeutic concentrations, $FFGen_3K(WHLPFKC)_{16}$ were able to expand the anti-angiogenic activity of iGG-MA hydrogel discs by not only preventing the formation of new EC sprouting, but also leading to their confined regression in the peri-implantar space. This level of control has fundamental importance for the regeneration of those tissues where angiogenesis needs to not be completely eliminated.

2. Materials and Methods

2.1. VEGF Blocker Synthesis and Characterisation

Poly-(ε-lysine) dendrons (Gen_3K) were synthesised with a di-phenylalanine core molecule (FF), a L-lysine core consisting of three levels of branching and a tethering with sixteen linear VEGF blocker peptide $(WHLPFKC)_{16}$ exposed at their uppermost branching generations as previously reported by Meikle *et al*. (2011). Briefly, the synthesis of both the linear WHLPFKC and the $FFGen_3K(WHLPFKC)_{16}$ started by coupling to a commercially-available resin for peptide synthesis an acid-labile Rink amide linker (0.4 mmol, Iris Biotech GmbH) later allowing the cleavage of the final product. Both types of peptidic aptamers were assembled by repeated coupling reactions, whereby each Fmoc-α-amine-protected amino acid unit (0.4 mmol, Novabiochem) was activated by 0.45 M O-Benzotriazole-N,N,N',N'-tetramethyluronium-hexafluoro-posphate (HBTU, Novabiochem) and 33 % (v/v) N,N-diisopropylethylamine (DIPEA, Sigma Aldrich Co. Ltd) and reacted at 60^0C for 5 minutes. At each step, the terminal amino acids were deprotected by removal of their Fmoc group by a 20 % (v/v) piperidine at 30^0C for 2 minutes. Following completion of the synthesis, peptides were purified using a standard semi-preparative HPLC method (Waters™ 717 plus Autosampler) performed on a hydrophobic RP 18 column (150x4.60 mm, Luna 3u C18 100 Å, Phenomenex) at 25^0C with a gradient mobile phase composed of a Solvent A (Deionised

water/0.1 % Trifluoroacetic Acid) and a Solvent B (Acetonitrile/0.1 % Trifluoroacetic acid). The eluate was visualised by UV light lamp at 230 nm (UVP Chromato-vue Cabinet). The collected peak fractions were identified by ESI-TOF mass spectrometry (Bruker microTOF).

2.2. Preparation of VEGF Blocker-Functionalised iGG-MA hydrogel discs

iGG-MA hydrogel discs were prepared according to an established protocol (Silva-Correia *et al*., 2011) where iGG-MA powder was initially dissolved with either WHLPFKC or $FFGen_3K(WHLPFKC)_{16}$ in distilled water at the final concentration of 2 % (w/v). Under continuous agitation at 42°C, a stable functionalised gellan gum solution was formed and deposited as droplets of 100 µL on the bottom of dry 24-well tissue culture plates (Fisher Scientific). The samples were left at 4°C overnight to allow the setting of the hydrogel. Non-functionalised iGG-MA hydrogel discs were prepared by the same procedure and used as control in all the experiments.

2.3. Endothelial Cell Sprouting 3D tests on Non- and Blocker-Functionalised iGG-MA hydrogels

HUVEC suspension ($3x10^4$cells/mL) (ATCC) was mixed with Matrigel™ (BD Biosciences) in ice-cold conditions in a total volume of 200 µL per well and rapidly pipetted onto the non- and VEGF blocker-modified iGG-MA drops ensuring the complete embedding of the hydrogels into the 3D matrix. After 30 minutes of incubation, the cells were treated with 1 mL of fresh endothelial basal medium (F-12K medium, PAA) containing 0.05 mg/mL of endothelial cell growth supplement (ECGS, Sigma Aldrich Co. Ltd), 0.1 mg/mL of heparin (Fisher Scientific) adjusted to a final concentration of 10% (v/v) of foetal bovine serum (FBS, PAA) for 24 and 48 hours at 37°C, under a 5% CO_2 and 95% air flow in a relative humidity condition. The ability of VEGF blocker dendrons to control capillary like-structure formation

was analysed by capturing images at 10x magnification from six different fields for each experimental well using a phase contrast microscopy (Nikon Eclipse TE2000-U) fitted with a digital camera (Nikon D1X). Whereas, to the purpose of monitoring the blocker release between iGG-MA and the surrounding Matrigel matrix, all samples were fixed with 4% (v/v) paraformaldehyde (Fisher Scientific) for 10 minutes at room temperature, followed by washing in water and staining with haematoxylin and eosin stain (H&E). Specimens were then observed under a phase contrast microscopy (Nikon Elipse TE 200U) and images captured using a digitised camera at 10 and 20x magnification (Canon LM Scope).

2.4. Quantitative Analysis of Endothelial Cell Sprouting

Due to the faster rate of diffusion of the linear form from the iGG-MA hydrogel mesh, quantitative analyses were performed on FFGen$_3$K (WHLPFKC)$_{16}$ – laden iGG-MA samples versus control ones.

Light microscopy images (8-bit) were analysed using a specific image-processing software, Image J/Analyze Skeleton (http://fiji.sc/AnalyzeSkeleton). The programme allowed the automated measurement of the mean value of sprouting length, number of free un- and associated termination points and junctions within an endothelial capillary-like network. This was obtained by skeletonising each EC sprout into a more compact representation while preserving the main features of the original image (Figure 1) (Valapala *et al*., 2011).

Based on the H&E-stained images (n=6), the number of EC nuclei per capillary-like structure was also counted after marking each nucleus as a black dot for easier identification and finally reported in an Excel file format.

2.5. CAM Model and Tissue Specimen Preparation

White fertilised chicken eggs (n=5, Pintobar, Portugal) were incubated at 37°C (Laboratory Incubator Series 8000, Termaks) for 3 days. Afterwards, albumen of 2.5 mL was extracted using a sterile syringe while the CAM of the fertilised egg was separated from the top part of the shell. This formed a small visible window (maximum of 15 mm in diameter) that allowed the easy evaluation and access to the CAM. The hole was sealed using a transparent tape (50x30 mm; BTK) to the purpose of preventing dehydration and any damage of the embryonic tissues. The eggs were placed at 3°C and 60% humidity until day 10 of embryonic development. At this time point, both non- and aptamer-functionalised iGG-MA discs were placed on the top of each CAM membrane. After 4 days of incubation, all CAM implants (n= 5 for each group) showing contact with host tissues were harvested and immediately fixed with 4% paraformaldehyde (Merck) for 10 minutes at -80°C. Samples were then dehydrated through a series of increasing ethanol (Fisher Scientific) concentrations for 2 hours and embedded in paraffin. The tissue blocks were allowed to cool for 2 hours and then carefully sectioned (5 μm) using a rotary microtome (Leica RM2135, Technologic Ltd). To promote tissue adhesion, the paraffin sections were mounted onto glass slides (VWR International Ltd) coated with 0.1% (w/v) gelatine (Aldrich-Sigma Ltd) and incubated at 60°C in an oven overnight.

2.6. Blood Vessel Identification by H&E and Lectin Staining

Paraffin sections were de-waxed with xylene (National Diagnostic) and ethanol (Fisher Scientific) for 10 minutes, followed by washing in water and by staining with hematoxylin (Sigma Aldrich Co. Ltd) for 6 minutes at room temperature. After washing under running tap water, sections were dehydrated in 90% (v/v) ethanol for 10 seconds, counterstained with eosin (Sigma Aldrich Co. Ltd) for 1 minute and dehydrated in a graded series of ethanol

rinses. Slides were soaked in 100% (v/v) ethanol and xylene for 3 minutes and then covered with a glass coverslip with DPX mounting medium (Fisher Scientific). Stained tissues were observed under a phase contrast microscopy (Nikon Elipse TE 200U) equipped with digital camera (Canon LM Scope) at 10 and x20 magnification. For lectin staining, tissue samples were treated with a solution of Fluorescein isothiocyanate (FITC)-conjugated lectin (Aldrich-Sigma Ltd) at the final concentration of 100 µg/mL and incubated in a humid chamber at 4°C overnight. Afterwards, all the slides (n=6) were carefully rinsed with distilled water and imaged using a confocal laser scanning microscopy (Leica UK), whereas signals were recorded in the green channel with an excitation 488 nm and emission 522 nm.

2.7. Morphometric Image Analysis

Morphometric image analysis was performed according to a published method (Gresta *et al*., 2014) whereby two hot spots at: i) central, and ii) iGG-MA interface regions of the surrounding tissue were identified and documented using an image analysis programme (Image J, http://rsb.info.nih.gov/ij/). Those areas were identified by dividing a single mosaic into a set of individual images (n=24) at a magnification of x10 and used for counting the number of blood vessels previously observed by phase contrast microscopy (Nikon Elipse TE 200U). The mean values of the vessel count were then divided by the hot spot area (in μm^2) and considered as microvessel density (MVD) as illustrated in Figure 2.

2.8. Statistical Analysis

All results from both *in vitro* and *in ovo* experiments were tested for statistical difference using one-way analysis of variance (ANOVA). A p value ≤ 0.05 was accepted as statistically significant for a 95% confidence interval while data were expressed as means ± standard deviation (SD).

3. Results

3.1. In vitro Sprouting Inhibition Test at the iGG-MA Material/Tissue Interface

The results showed that iGG-MA hydrogel discs prevented EC tube infiltration (Figure 3). However, when the hydrogels were functionalised with both linear and VEGF blocker dendrons their anti-angiogenic capacity to inhibit HUVEC sprouting formation was expanded to the surrounding tissue and, in the case of the VEGF blocker dendron, confined to the iGG-MA/tissue boundary after both 24 and 48 hours incubation (Figure 3, dashed lines). Instead, a more extended area of inhibition was observed in the case of hydrogels pre-loaded with linear WHLPFKC in which a relatively rapid diffusion of the peptides from the iGG-MA hydrogel discs to the surrounding Matrigel led to an inhibition of the sprouting already after 24 hours (Figure 3, grey arrows). This trend was more pronounced at 48 hours compared to that of $FFGen_3K(WHLPFKC)_{16}$ where inhibition was limited to the iGG-MA/Matrigel interface (Figure 3, white arrows). At the same experimental points, the non-modified control material interface showed to be colonised by a well-organised and compacted network of capillary-like structures at 24 and 48 hours after plating (Figure 3, black arrows).

The pattern of controlled angiogenesis in the VEGF blocker–modified iGG-MA hydrogel discs was confirmed by the H&E staining of the samples (Figure 4). An uptake of staining by the scaffold allowed the clear identification of the material boundary (Figure 4, dashed lines), thus showing the degree of contact between its surface and the capillary-like network in both the non- and aptamer-functionalised hydrogel discs. Noticeably, extented sprouting covered the whole area of inspection and clear contacts with the iGG-MA surface was observed in the control (Figure 4, black circle) as opposed to those samples loaded with both linear and dendron VEGF blockers (Figure 4, white arrows). In $FFGen_3K(WHLPFKC)_{16}$–modified iGG-MA hydrogel discs, the formation of pre-existing tubular structures around the hydrogel

surface appeared to regress after 48 hours of incubation (Figure 4, white arrows). Figure 5 (A) shows a reduction in the average number of branching points 4.71±1.62 μm^2 (control iGG-MA = 6.93±1.69 μm^2) and associated to a higher number of free unassociated points 3.12±2.68 μm^2 (control iGG-MA samples= 0.95±0.74 μm^2) (Figure 5 A). Similar results were observed in terms of the number of junctions [un-treated iGG-MA samples = 9.13±1.24 μm^2; functionalised iGG-MA samples = 2.77±1.65 μm^2] (Figure 5 B) with no significant difference in the total average of branch length [un-treated iGG-MA samples = 24.43±2.26 μm^2; functionalised iGG-MA samples = 22.26±4.14 μm^2] (Figure 5 C). There was no significant difference in the total number of cells between non- [385±86.7 cells/field] and dendron-laden iGG-MA hydrogel discs [289±87.8 cells/field] at the tissue/iGG-MA interface, respectively (Figure 5 D).

3.2. CAM of iGG-MA and Dendron-laden iGG-MA Hydrogel Discs

Both non- and aptamer -laden iGG-MA hydrogel discs were well-tolerated by the host tissue membrane after implantation as no necrosis or significant host response was detected. Light microscopy analysis of the non-treated samples revealed the presence of elongated blood vessels that longitudinally converged towards the material at the tissue/iGG-MA interface (Figure 6 A, black arrows). These appeared sinusoidal and uniformly dilated (Figure 6 A, black circle) when compared to the $FFGen_3K(WHLPFK)_{16}$-laden iGG-MA samples. Indeed, this active angiogenesis process was not observed in aptamer-laden iGG-MA samples whereby capillaries were irregularly shaped (Figure 6 A, white arrows), smaller and clustered after 4 days of implantation (Figure 6 A, white dashed circle on black background).

Similar anti-angiogenic effects of VEGF blocker dendrons were observed in sections stained with lectin as illustrated in Figure 6 B. A large number of sizable and elongated blood vessels, which were oriented parallel along the length of the iGG-MA hydrogel perimeter,

were detected only in the control samples (Figure 6 B, black arrows). Such enhanced organisation was lost in the presence of $FFGen_3K(WHLPFKC)_{16}$, which promoted growth of smaller (Figure 6 B, white dashed circle on black background) and convoluted (Figure 6 B, white arrows) capillaries that were either far or randomly distributed at the tissue/iGG-MA interface (Figure 6 B, dashed lines) at days 4 implantation.

Figure 7 shows MVD and a decreased number of blood vessels within the $FFGen_3K(WHLPFKC)_{16}$-laden iGG-MA samples (16±2.8 vessels/μm^2) when compared to the control hydrogels (48±3.4 vessels/μm^2). However, MVD values showed a similar trend in the central areas (untreated iGG-MA samples = 150±1.2 vessels/μm^2; $FFGen_3K(WHLPFKC)_{16}$-functionalised iGG-MA samples =135± 3.2 vessels/μm^2) of the two tested samples as illustrated in Figure 7 A. Moreover, the total number of blood vessels was found to be similar throughtout the tissue undergoing the implants of both non- and -functionalised hydrogels (Figure 7 B).

4. Discussion

A known VEGF blocker sequence has been integrated at the uppermost branching generation of dendrons that have specifically been designed to enhance availability of the biospecific aptamers and to improve retention in and controlled delivery from hydrogels for tissue engineering. The tailor-made design had already shown the clinical potential of this novel class of aptamers (Meikle *et al*., 2011). They were based on the amino acid lysine which contains an alkyl amino side-chain capable to allow the branching into a larger macromolecule with an overall structure presenting the biospecific sequences at relatively high density and in an orderly-spaced manner to the surrounding biological micro-environment. This type of dendron was assembled using a new microwave-assisted SPPS

method that offered speed and high yield of reaction and ultimately an effective control over the synthesis of the FF-$Gen_3K(WHLPFKC)_{16}$. Such dendrons have been synthesised to have a root of FF capable of preferentially interacting with macromolecules of the tissue extracellular matrix (i.e. collagen) and an hyperbranched structure or protein scaffold capable to expose an increased density of anti-angiogenic peptide sequence (WHLPFKC) at their uppermost branching generation (Meikle *et al*., 2011). WHLPFKC has been recently isolated by phage display technique (Erdag *et al*., 2007) and demonstrated to be capable of establishing a bond with human $VEGF_{165}$ at molar ratio of 1:1 even in presence of both Type I and II collagen [our unpublished data]. Forming a stable complex with the angiogenic growth factor, this linear peptide essentially antagonised the autocrine VEGF effects on HUVECs *in vitro*. However, when grafted to a dendron scaffold, its bioavailability and biological actvity was successfully maximised providing evidence for the control of proliferation and regression of capillary-like structures in HUVECs. Moreover, the relatively hydrophobic nature of these VEGF blocker dendrons enhances their potential to penetrate collagenous matrices and to revert angiogenesis in absence of cytotoxicity (Meikle *et al*., 2011). On the basis of this evidence, the tailored-design of the material in the present study enabled a control over the release of VEGF blocker sequences by: (i) reducing the problem of burst release from the gel associated with the relatively smaller linear aptamer through an increase of the molecular weight and through the enhancement of physical interactions between the di-phenylalanine groups at the root of the dendrons and the methacrylate hydrophobic residues of the iGG-MA and (ii) increasing the density and space distribution of the aptamer through the exposure of sixteen units per dendrimer. Although specific rheological studies were not investigated in this paper, it was observed that the hydrogel formed a more compact structure when dendrons were encapsulated in it supporting the occurrence of hydrophobic interaction within the gel mesh. This more compact structure of

the hydrogel could also have played a role in limiting the release of the VEGF blocker dendrons. The overall outcome is the significant clinical advantage of having the anti-angiogenic effect circumscribed to the immediate surrounding of the implant. Indeed, the contrast phase microscopy analysis demonstrated that, when compared to the non-modified iGG-MA, the FF-$Gen_3K(WHLPFKC)_{16}$ -laden biomaterial induced a regression of the capillary-like structures typical of the Matrigel endothelial sprouting assay only at the hydrogel boundary. Contrariwise, a more pronounced area of inhibition could be observed in the case of the biomaterial where the linear peptide had been entrapped. At cellular level, this effect can be attributed to cell apoptosis in absence of sufficient levels of VEGF as the microscopy highlighted morphological changes with HUVECs showing blebbing and round-shaped morphology. Altogether these data indicate the efficiency of the VEGF blocker dendrons in inhibiting the endothelial sprouting from existing capillary-like structures which is known to be strictly dependent on VEGF-related activity (Ahmad *et al*., 2011) and suggest a potential advantage in clinical applications such as the regeneration of the nucleous pulposus of the intervertebral disc where the formation of new avascular tissue needs to coexhist with the vascularised annulus fibrosus.

The data obtained by the *in ovo* model supported the findings of the *in vitro* study and added more information related to the effect of the VEGF blocker dendron release on a highly vascularised tissue such as the chorioallontoic membrane surrounding the chick embryo. Both control and aptamer-functionalised iGG-MA hydrogel discs prevented blood vessel infiltration mainly because of the relatively tight structure of the gel mesh. However, those samples that had been modified by the encapsulation of the VEGF blocker dendron allows the formation only of thinner and rounded vessels that failed to develop especially at the tissue/iGG-MA interface in a manner similar to the regression by cell blebbing and rounding

observed *in vitro* and in line with other studies demonstrating the key role of VEGF concentration gradients in angiogenesis (Shamloo *et al*., 2012). The qualitatively-assessed reduction in MVD at the boundary of aptamer-functionalised iGG-MA samples, but not in the central areas, is corroborated by previous work showing similar findings in cases where vessel morphology and size changed with interferences in the local VEGF concentration levels (Ozawa *et al*., 2004). These authors found that low VEGF expression induced destabilised retinal capillaries gradually regressing rather than progressing into angiogenesis. The disruption of the interaction of the VEGF molecule with its receptor on the endothelial cell membrane appeared to be one of the determinants in this critical event (Nakatsu *et al*., 2003). Although in our results the average number of capillaries was not significantly different between analysed samples, recent genetic studies in mice have reported that targeting blood vessel function and stabilisation, rather than their numbers, may provide an alternative approach to prevent angiogenesis in tissue regeneration (Loges *et al*., 2010; Alvarez *et al*., 2009).

5. Conclusions

In this study, FF-$Gen_3K(WHLPFKC)_{16}$ showed to represent a potentially useful biofunctionalisation strategy to enhance the clinical performance of cartilage tissue engineering based on iGG-MA hydrogel discs. The fine control of angiogenesis around the gel boundary is likely to impede the invasion of blood vessels from the surrounding vascularised tissue independently from its tight mesh. As the biomaterial is absorbed and new tissue is formed, it is likely that angiogenesis will not overcome avascular cartilage as its penetration will no longer be stopped by the tight mesh, but rather by the sustained but circubscribed release of the aptamer; a property that cannot be achieved by the use of the small molecular weight, linear VEGF blocker WHLPFKC.

Acknowledgments

This work was mainly supported by the EC FP7 project Disc Regeneration (Contract No NMP3-LA-2008-213904). This study was also funded by the EC FP7 Programme contract agreement no REGPOT-CT2012-316331-POLARIS.

References

Ahmad S, Hewett PW, Al-Ani B, Sissaoui S, Fujisawa T, Cudmore MJ, Ahmed A. 2011, Autocrine activity of soluble Flt-1 controls endothelial cell function and angiogenesis, *Vasc Cell*, **3**: 15

Al-Jamal KT, Al-Jamal WT, Akerman S, Podesta JE, Yilmazer A, Turton JA, Bianco A, Vargesson N, Kanthou C, Florence AT, Tozer GM, Kostarelos K. 2010, Systemic antiangiogenic activity of cationic poly-L-lysine dendrimer delays tumor growth, *Proc Natl Acad Sci U S A*, **107**: 3966-3971

Alvarez Y, Astudillo O, Jensen L, Reynolds AL, Waghorne N, Brazil DP, Cao Y, O'Connor JJ, Kennedy BN. 2009, Selective inhibition of retinal angiogenesis by targeting PI3 kinase, *PLoS One*, **4**: e7867

Bischoff J, Griffioen AW. 2008, In memoriam Dr. Judah Folkman, *Angiogenesis*, **11**: 1-2

Bonnet CS, Walsh DA. 2005, Osteoarthritis, angiogenesis and inflammation, *Rheumatology (Oxford)*, **44**: 7-16

Bunka DH, Stockley PG. 2006, Aptamers come of age - at last, *Nat Rev Microbiol*, **4**: 588-596

Carmeliet P. 2003, Angiogenesis in health and disease, *Nat Med*, **9**: 653-660

Dahners LE, Mullis BH. 2004, Effects of nonsteroidal anti-inflammatory drugs on bone formation and soft-tissue healing, *J Am Acad Orthop Surg*, **12**: 139-143

Erdag B, Balcioglu KB, Kumbasar A, Celikbicak O, Zeder-Lutz G, Altschuh D, Salih B, Baysal K. 2007, Novel short peptides isolated from phage display library inhibit vascular endothelial growth factor activity, *Mol Biotechnol*, **35**: 51-63

Gresta LT, Rodrigues Jr IA, Cabral MMDA. 2014, Microvessel Density Quantification in Gastric Cancer: Comparing Methods for Standard Measures, *J Cancer Sci Ther*, **6**:401-405

Kasai S, Nagasawa H, Shimamura M, Uto Y, Hori H. 2002, Design and synthesis of antiangiogenic/heparin-binding arginine dendrimer mimicking the surface of endostatin, *Bioorg Med Chem Lett*, **12**: 951-954

Kim SH, Turnbull J, Guimond S. 2011, Extracellular matrix and cell signalling: the dynamic cooperation of integrin, proteoglycan and growth factor receptor, *J Endocrinol*, **209**: 139-151

Li WS, Aida T. 2009, Dendrimer porphyrins and phthalocyanines, *Chem Rev*, **109**: 6047-6076

Lien S, Lowman HB. 2003, Therapeutic peptides, *Trends Biotechnol*, **21**: 556-562

Loges S, Schmidt T, Carmeliet P. 2010, Mechanisms of resistance to anti-angiogenic therapy and development of third-generation anti-angiogenic drug candidates, *Genes Cancer*, **1**: 12-25

Meikle ST, Perugini V, Guildford AL, Santin M. 2011, Synthesis, characterisation and in vitro anti-angiogenic potential of dendron VEGF blockers, *Macromol Biosci*, **11**: 1761-1765

Menjoge AR, Kannan RM, Tomalia DA. 2010, Dendrimer-based drug and imaging conjugates: design considerations for nanomedical applications, *Drug Discov Today*, **15**: 171-185

Nakatsu MN, Sainson RC, Perez-del-Pulgar S, Aoto JN, Aitkenhead M, Taylor KL, Carpenter PM, Hughes CC. 2003, VEGF(121) and VEGF(165) regulate blood vessel diameter through vascular endothelial growth factor receptor 2 in an in vitro angiogenesis model, *Lab Invest*, **83**: 1873-1885

Nugent HM, Edelman ER. 2003, Tissue engineering therapy for cardiovascular disease, *Circ Res*, **92**: 1068-1078

Ozawa CR, Banfi A, Glazer NL, Thurston G, Springer ML, Kraft PE, McDonald DM, Blau HM. 2004, Microenvironmental VEGF concentration, not total dose, determines a threshold between normal and aberrant angiogenesis, *J Clin Invest*, **113**: 516-527

Pednekar PP, Jadhav KR, Kadam VJ. 2012, Aptamer-dendrimer bioconjugate: a nanotool for therapeutics, diagnosis, and imaging, *Expert Opin Drug Deliv*, **9**: 1273-1288

Pereira DR, Canadas RF, Silva-Correia J, Marques AP, Reis RL, Oliveira JM. 2014, Gellan gum-based Hydrogel Bilayered Scaffolds for Osteochondral Tissue Engineering - BIOCERAMICS 25. *Key Eng Mater*, **587**: 255-260

Pulsatelli L, Addimanda O, Brusi V, Pavloska B, Meliconi R. 2013, New findings in osteoarthritis pathogenesis: therapeutic implications, *Ther Adv Chronic Dis*, **4**: 23-43

Reitmaier S, Kreja L, Gruchenberg K, Kanter B, Silva-Correia J, Oliveira JM, Reis RL, Perugini V, Santin M, Ignatius A., Wilke HJ. 2014, In vivo biofunctional evaluation of hydrogels for disc regeneration, *Eur Spine J*, **23**: 19-26

Shamloo A, Xu H, Heilshorn S. 2012, Mechanisms of vascular endothelial growth factor-induced pathfinding by endothelial sprouts in biomaterials, *Tissue Eng Part A*, **18**: 320-330

Shaunak S, Thomas S, Gianasi E, Godwin A, Jones E, Teo I, Mireskandari K, Luthert P, Duncan R, Patterson S, Khaw P, Brocchini S. 2004, Polyvalent dendrimer glucosamine conjugates prevent scar tissue formation, *Nat Biotechnol*, **22**: 977-984

Silva-Correia J, Oliveira JM, Caridade SG, Oliveira JT, Sousa RA, Mano JF, Reis RL. 2011, Gellan gum-based hydrogels for intervertebral disc tissue-engineering applications, *J Tissue Eng Regen Med*, **5**: e97-107

Silva-Correia J, Pereira H, Yan LP, Miranda-Gonçalves V, Oliveira AL, Oliveira JM, Reis RM, Espregueira-Mendes JD, Reis RL. 2012a, Advanced mimetic materials for meniscus tissue engineering: targeting segmental vascularization, *J Tissue Eng Regen Med*, **6**: 18

Silva-Correia J, Gloria A, Oliveira MB, Mano JF, Oliveira JM, Ambrosio L, Reis RL. 2013a, Rheological and Mechanical Properties of Acellular and Cell-laden Methacrylated Gellan Gum Hydrogels, *J Biomed Mater Res Part A*, **101**: 3438-3446

Silva-Correia J, Zavan B, Vindigni V, Silva TH, Oliveira JM, Abatangelo G, Reis RL. 2013b, Biocompatibility Evaluation of Ionic- and Photo-Crosslinked Methacrylated Gellan Gum Hydrogels: In Vitro and In Vivo Study, *Adv Healthc Mater*, **2**: 568-575

Silva-Correia J, Miranda-Gonçalves V, Salgado AJ, Sousa N, Oliveira JM, Reis RM, Reis RL. 2012b, Angiogenic potential of gellan-gum-based hydrogels for application in nucleus pulposus regeneration: in vivo study, *Tissue Eng Part A*, **18**: 1203-1212

Skerra A. 2007, Alternative non-antibody scaffolds for molecular recognition, *Curr Opin Biotechnol*, **18**: 295-304

Song KM, Lee S, Ban C. 2012, Aptamers and their biological applications, *Sensors (Basel)*, **12**: 612-631

Tomalia DA. 2009, In quest of a systematic framework for unifying and defining nanoscience, *J Nanopart Res*, **11**: 1251-1310

Tomalia DA. 1991, Dendrimer research, *Science*, **252**: 1231

Troken A, Marion N, Hollister S, Mao J. 2007, Tissue engineering of the synovial joint: the role of cell density, *Proc Inst Mech Eng H*, **221**: 429-440

Trujillo CA, Nery AA, Alves JM, Martins AH, Ulrich H. 2007, Development of the anti-VEGF aptamer to a therapeutic agent for clinical ophthalmology, *Clin Ophthalmol*, **1**: 393-402

Tuerk C, Gold L. 1990, Systematic evolution of ligands by exponential enrichment: RNA ligands to bacteriophage T4 DNA polymerase, *Science*, **249**: 505-510

Valapala M, Thamake SI, Vishwanatha JK. 2011, A competitive hexapeptide inhibitor of annexin A2 prevents hypoxia-induced angiogenic events, *J Cell Sci*, **124**: 1453-1464

Vincent L, Varet J, Pille JY, Bompais H, Opolon P, Maksimenko A, Malvy C, Mirshahi M, Lu H, Vannier JP, Soria C, Li H. 2003, Efficacy of dendrimer-mediated angiostatin and TIMP-2 gene delivery on inhibition of tumor growth and angiogenesis: in vitro and in vivo studies, *Int J Cancer*, **105**: 419-429

Vinores SA. 2006, Pegaptanib in the treatment of wet, age-related macular degeneration, *Int J Nanomedicine*, **1**: 263-268

Wang M. 2003, Developing bioactive composite materials for tissue replacement, *Biomaterials*, **24**: 2133-2151

Xu X, Weng Y, Xu L, Chen H. 2013, Sustained release of Avastin® from polysaccharides cross-linked hydrogels for ocular drug delivery, *Int J Biol Macromol*, **60**: 272-276

Figure Captions

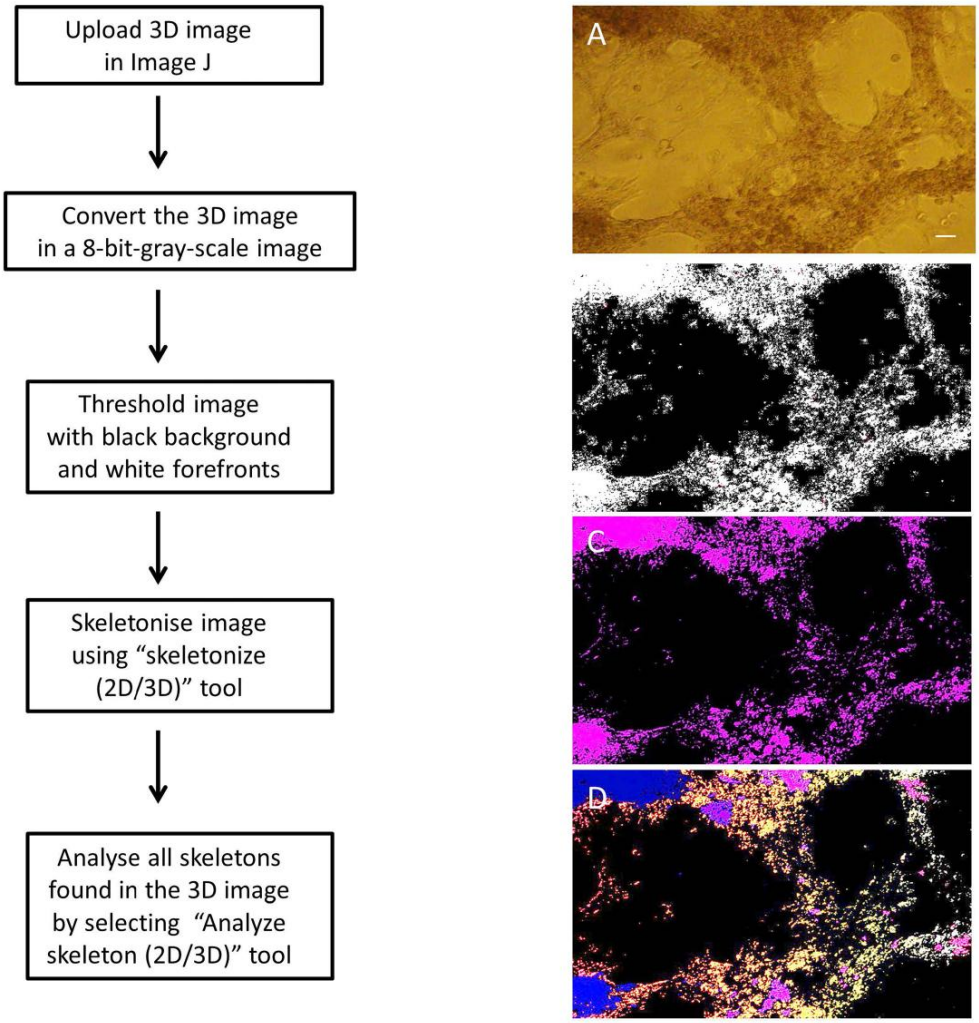

Figure 1. Steps of image preparation (Left panel) and HUVEC tube identification (Right panel) using a skeletonised method by Image J (Valapala *et al*., 2011). (A) An original image was initially, (B) skeletonised by highlighting EC tubes in white running over a black background, (C) tagged for pointing out the "positive" tube structures (purple), and (D) assessed with regards branch points and length (orange/white) free un-associated points (purple) and actual junctions (blue) between EC tubes. Scale bar is 50 µm.

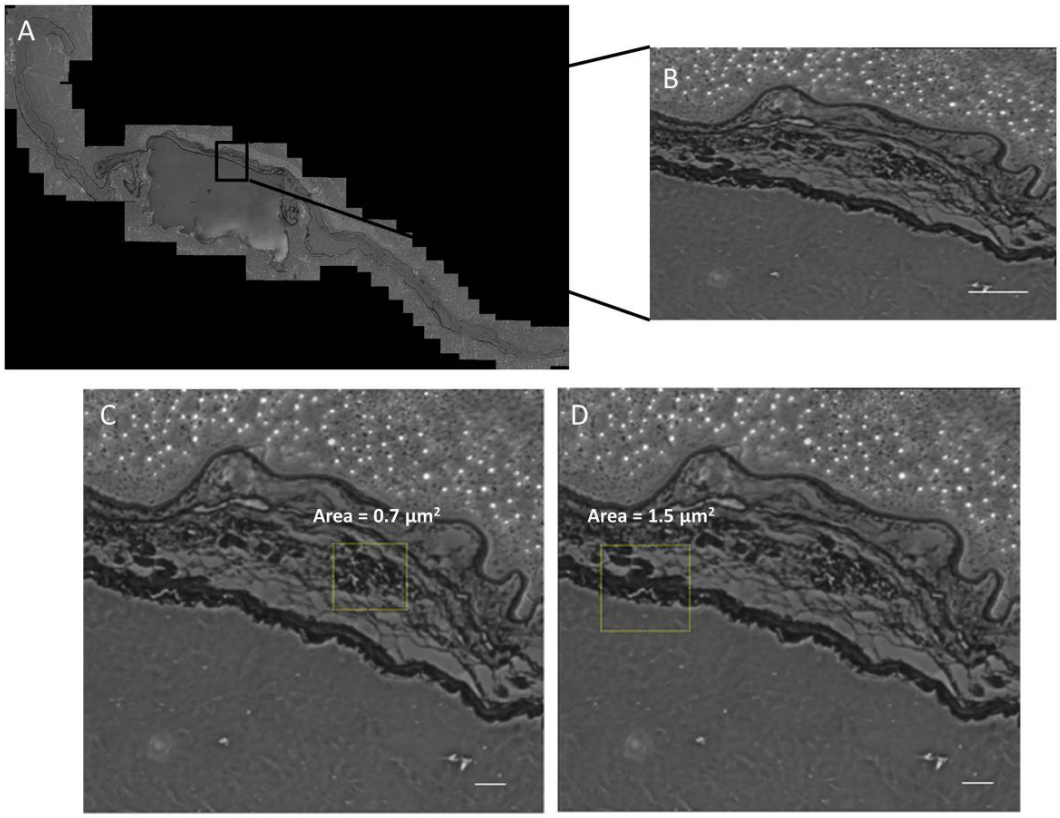

Figure 2. Example of blood vessel analysis and quantification. (A) A mosaic image was morphometrically analysed by dividing the (B) individual sections into two distinct hot spots located at the (C) centre and (D) iGG-MA interface of the tested tissues. Scale bar is 300 and 150 µm.

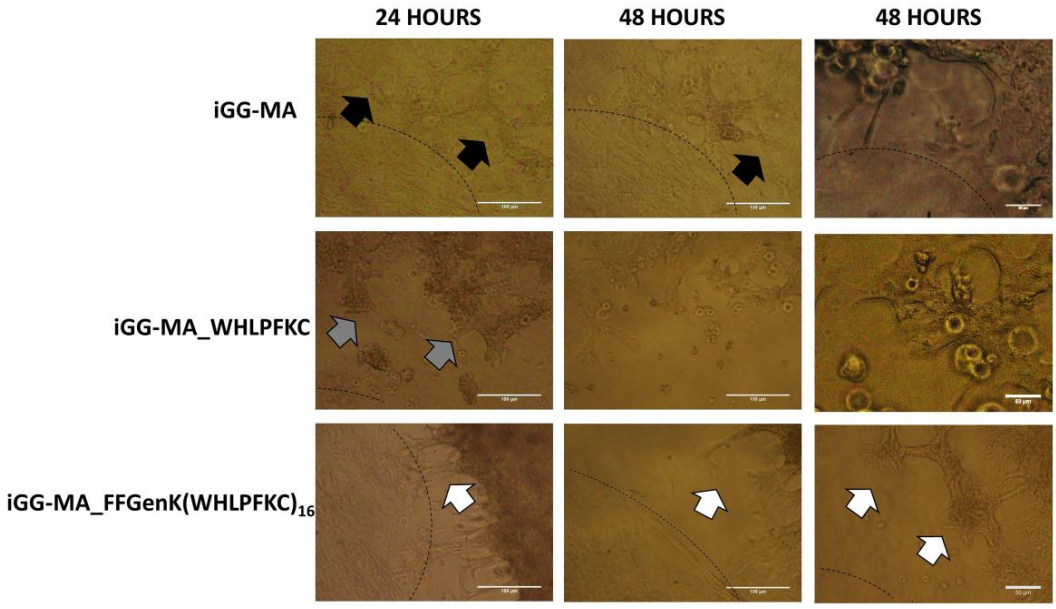

Figure 3. Effect of VEGF blockers integrated in iGG-MA hydrogel discs on the formation of HUVEC tubes at 24 and 48 hours. Dashed lines indicate the approximate position of the iGG-MA hydrogel discs; grey and whitearrows point out the capacity of both WHLPFKC and $FFGen_3K(WHLPFKC)_{16}$ to induce an EC sprouting inhibition at the iGG-MA boundary when compared to the control (black arrows). Scale bar is 100 and 50 μm.

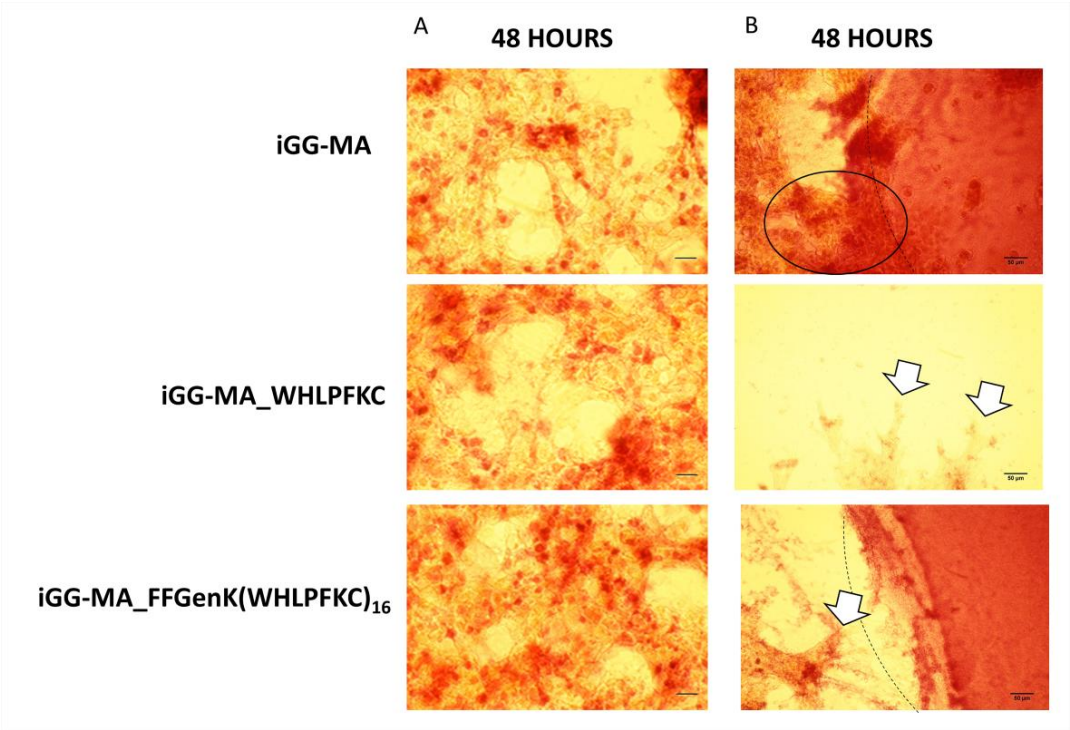

Figure 4. H&E staining of both untreated and functionalised iGG-MA samples. (A) centre; (B) iGG-MA interface. Circle evidences contacts between iGG-MA boundary and the tube network while white arrows indicate an area of capillary-like structures in phase of regression at the biomaterial interface (dashed lines). Scale bar is 50 µm.

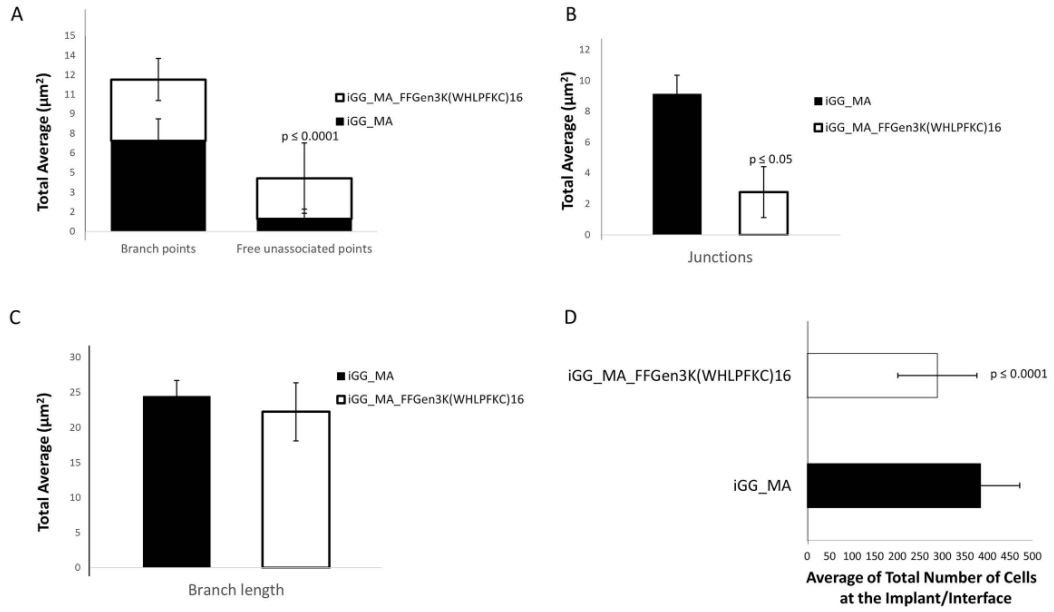

Figure 5. HUVEC tube analysis and quantification of both tested samples. (A) Average of number of branch and free un-associated points; (B) total of junctions; (C) branch length and (D) number of cells associated with HUVEC tubes at the biomaterial interface. (n=6).

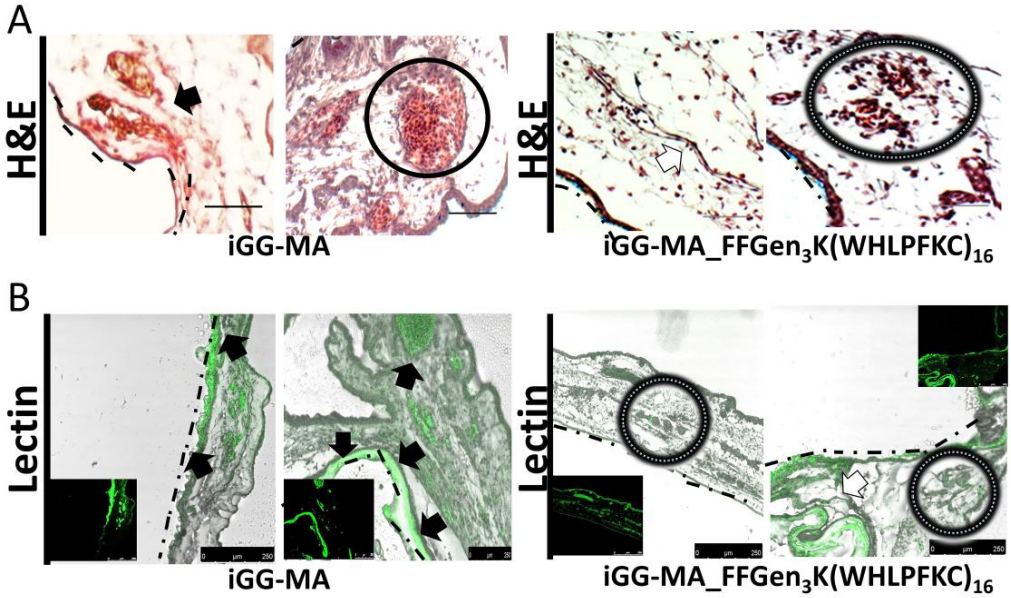

Figure 6. Functionalised iGG-MA hydrogel discs showed ability to affect blood vessel maintenance. (A) H&E, and (B) lectin staining. Blood vessels of regular shape and size were found to longitudinally run towards the biomaterial boundary only in the control samples (black arrows). Such activity was completely lost in presence of $FFGen_3K$ $(WHLPFKC)_{16}$ whereby capillaries appeared tortuous (white arrows), clustered (white dashed circle on black background) and either far or irregularly distributed at the biomaterial interface (dashed lines). Scale bar is 50 and 250 μm.

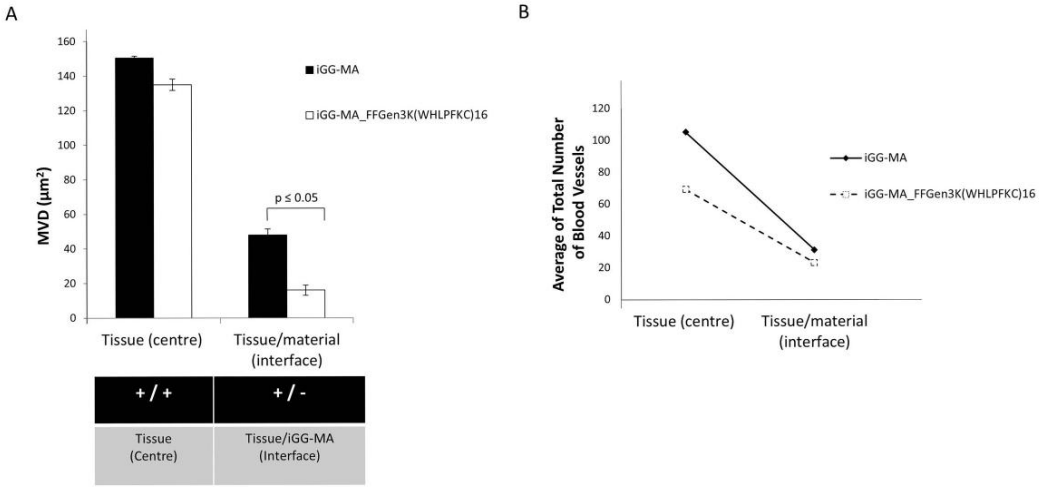

Figure 7. Quantification of both MVD and number of blood vessels within the non- and treated iGG-MA samples. Changes in (A) MVD values associated with higher, and (B) number of capillaries were found throughout of the control compared to the iGG-MA with $FFGen_3K(WHLPFKC)_{16}$. (n=24).